

# Charge asymmetries in $\gamma\gamma \rightarrow \ell^+\ell^- + \nu$ 's ( $\ell = \mu, e$ ) with polarized photons in the Standard Model.

D. A. Anipko,<sup>1</sup> M. Cannoni,<sup>2,3</sup> I. F. Ginzburg,<sup>1</sup> K. A. Kanishev,<sup>1,4</sup> A. V. Pak,<sup>1,5</sup> and O. Panella<sup>3</sup>

<sup>1</sup>*Sobolev Institute of Mathematics and Novosibirsk State University, Novosibirsk, 630090, Russia*

<sup>2</sup>*Università di Perugia, Dipartimento di Fisica, Via A. Pascoli, I-06123, Perugia, Italy*

<sup>3</sup>*Istituto Nazionale di Fisica Nucleare, Sezione di Perugia, Via A. Pascoli, I-06123, Perugia, Italy*

<sup>4</sup>*University of Warsaw, 00-681 Warsaw, Poland*

<sup>5</sup>*Department of Physics, University of Alberta, Edmonton, AB T6G 2G7, Canada*

(Dated: 10/6/2008)

## Abstract

It is shown that in reaction  $\gamma\gamma \rightarrow \ell^+\ell^- + \nu$ 's at  $\sqrt{s} > 200$  GeV with polarized photons, large and well observable differences arise in the distribution of positive and negative charged leptons ( $\ell = \mu^\pm, e^\pm$ ), (charge asymmetry). The modification due to the contribution of the cascade processes with intermediate  $\tau$ -lepton in  $\gamma\gamma \rightarrow W^\pm\ell^\mp + \nu$ 's reaction is taken into account. This charge asymmetry is potentially sensitive to effects of physics beyond the standard model at the anticipated luminosity of the Photon Collider mode of the future international linear collider.

## I. INTRODUCTION

The Photon Collider (PC) option of the planned International Linear Collider (ILC) (see e.g. [1], [2]) will offer a specific window for the study of new effects in both Standard Model (SM) and New Physics. In particular, it is expected that the charge asymmetry of leptons, produced in the collision of *neutral but highly polarized colliding particles*  $\gamma\gamma \rightarrow \ell^+\ell^- + \text{neutrals}$  (where  $\ell = \mu, e$ ), can be a good tool for the discovery of New Physics effects. With this aim the study of such asymmetry in SM is a necessary step for both better knowledge of SM and understanding of background for New Physics effects.

In this paper we study the SM process, in which *neutrals* are neutrinos and the main (but not single) mechanism for charged lepton production is given by  $\gamma\gamma \rightarrow W^+W^-$  process with subsequent lepton decay of  $W$ . The latter process,  $\sigma(\gamma\gamma \rightarrow WW)Br(W \rightarrow \mu\nu) = 8.8$  pb, will ensure very high event rate at the anticipated integrated luminosity of ILC ( $100 \text{ fb}^{-1}$ ), about  $10^6$  events per year. The charge asymmetry here appears due to transformation of initial photon helicity into distribution of final leptons via P-violating but CP-preserving leptonic decay of  $W$ . In the following we consider the particular case  $\ell = \mu$  for definiteness. The considered effects are identical for electrons and muons. So that, absolutely the same asymmetry will be observed in  $e^+e^-$ ,  $e^+\mu^-$ ,  $\mu^+e^-$  distributions. All these contributions should be added for a complete analysis. This will enhance the value of the cross section for  $\gamma\gamma \rightarrow \mu^+\mu^- + \nu$ 's from 1.2 to 4.8 pb.

In the main body of the paper we consider the collision of a photon with helicity  $\lambda_1$  moving in the positive direction of the  $z$  axis with a photon of helicity  $\lambda_2$  moving in the opposite direction. This initial state is denoted as  $\gamma_{\lambda_1}\gamma_{\lambda_2}$  with  $\lambda_i = \pm$  (left or right circular polarization). For example, the initial state with  $\lambda_1 = +1$ ,  $\lambda_2 = -1$  is written as  $\gamma_+\gamma_-$ . With this choice of the positive direction of the  $z$  axis we define the longitudinal momentum  $p_{\parallel} \equiv p_z$  and the transverse mo-

mentum  $p_{\perp} \equiv \sqrt{p_x^2 + p_y^2}$ . For definiteness, we present most of the results for monochromatic photon beams at  $\sqrt{s}_{\gamma\gamma} = 500$  GeV ( $E_{\gamma} = 250$  GeV). The above definitions will be slightly modified when discussing the effects due to the non-monochromaticity of photon beams in the future Photon Collider. We start our numerical calculations with the CompHEP package [3] and then switch to the CalcHEP package [4] which allows one to take into account the circular polarization of the initial photons and choose different random seed numbers for the Monte Carlo (MC) generator which is necessary for an estimate of the statistical inaccuracy of future experiments.

The observable final state with  $W + \mu$  or two muons with missing transverse momentum carried away by neutrinos can appear either via processes

$$\gamma\gamma \rightarrow W\mu\nu \quad (\gamma\gamma \rightarrow \mu^+\mu^-\nu_{\mu}\bar{\nu}_{\mu}), \quad (1)$$

or via *cascade processes* like:

$$\gamma\gamma \rightarrow W^+\bar{\nu}_{\tau} \quad \begin{array}{c} \tau^- \\ \downarrow \\ \mu^-\bar{\nu}_{\mu}\nu_{\tau} \end{array} = W^+\bar{\nu}_{\tau}\mu^-\bar{\nu}_{\mu}\nu_{\tau} \quad (2)$$

$$\gamma\gamma \rightarrow \tau^-\bar{\nu}_{\tau}\nu_{\tau} \quad \begin{array}{c} \tau^+ \\ \downarrow \\ \mu^+\nu_{\mu}\bar{\nu}_{\tau} \end{array} = \mu^-\mu^+\bar{\nu}_{\mu}\nu_{\tau}\nu_{\mu}\bar{\nu}_{\tau} \quad \bar{\nu}_{\tau}\nu_{\tau}, \quad (3)$$

in which six or eight particles are present in the final state.

To reduce CPU time in the Monte Carlo event generation,  $10^6$  events for each channel, we obtain the essential part of the results for the  $\gamma\gamma \rightarrow W^\pm\mu^\mp + \nu$ 's process, not taking into account issues related to the reconstruction of the  $W$ . The analysis of this process allows us to extract the main features of the effect of interest, i.e. the difference in the distributions of  $\mu^+$  and  $\mu^-$  at fixed photon helicities (*global charge asymmetry*). We show that the additional diagrams that contribute to  $\gamma\gamma \rightarrow \ell^+\ell^- + \text{neutrals}$  give negligible contribution to the cross section and charge asymmetry.

We start with the description in Section II of the general features of the effect, neglecting cascade processes. We classify the diagrams contributing to  $\gamma\gamma \rightarrow W\mu\nu$  and  $\gamma\gamma \rightarrow \mu^+\mu^-\nu_\mu\bar{\nu}_\mu$  according to the different topologies and give an approximate analytical estimate of their relative impact on the cross section (Sec. II A). These estimates allow us to present qualitative explanation of the appearance of the charge asymmetry (Sec. II B).

We then introduce suitable variables for the description of the *global asymmetry*, i.e. the difference in distributions of  $\mu^+$  and  $\mu^-$  in the processes  $\gamma\gamma \rightarrow W^\pm\mu^\pm + \nu$ 's or  $\gamma\gamma \rightarrow \mu^+\mu^- + \nu$ 's (Sec. II D). In this very section we describe the cuts applied to the observed particles. In Sec. II E we discuss a computational method used to estimate a lower bound on the statistical uncertainty of future experiments. This estimate is obtained directly by the repeated Monte Carlo simulations with an anticipated number of events.

Section III is devoted to detailed description of the global charge asymmetry of leptons in the process  $\gamma\gamma \rightarrow W\mu\nu$  in monochromatic  $\gamma\gamma$  collisions.

The accurate calculation of cascade processes with six or more particles in the final state is a computationally challenging task with available software. Since we use CompHEP/CalcHEP packages which don't fix the helicity of final states while the discussed effects strongly depend on the helicity, the direct use of existing software for tau decay simulation like TAUOLA [5] is not possible here. In Sec. IV we construct reasonable approximations in the description of cascade processes (3). The detailed analysis of the modification of momentum distributions allows to find that the inaccuracy implemented by the mentioned approximation in the final result is within the estimated statistical uncertainty of future experiments.

In Sec. V we discuss the total observable asymmetries.

High energy photons will be produced at the Photon Collider through Compton back-scattering of laser photons from high energy electron or (and) positron beams: the photons will not be monochromatic but will demonstrate an energy and polarization distribution. The high energy part of this spectrum will mainly include photons with definite helicity  $\lambda_i$  close to  $\pm 1$  [2]. We analyse the influence of initial photon non-monochromaticity on results in Sec. VI.

The *correlative asymmetry* in  $\mu^+$  and  $\mu^-$  momenta in each event of  $\gamma\gamma \rightarrow \mu^+\mu^- + \nu$ 's is expected to provide more information in the search for effects of physics beyond the SM. We discuss it in Sec. VII.

We conclude and summarize the obtained results in Sec. VIII.

Preliminary (and incomplete) parts of this work were reported earlier [6].

## II. GENERAL FEATURES

The SM cross section of  $\gamma\gamma \rightarrow W^+W^-$  at center of mass energy greater than 200 GeV remains almost con-

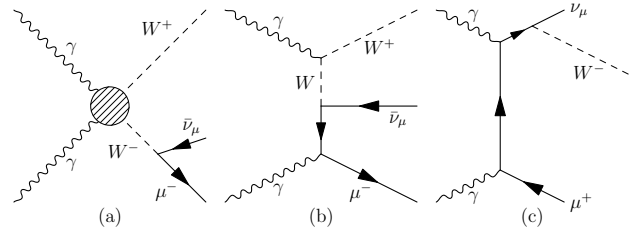


FIG. 1: Classes of tree level Feynman diagrams contributing to  $\gamma\gamma \rightarrow W^+\mu^-\bar{\nu}$ , (a-c). The grey blob in (a) represents diagrams with  $W$  exchange with trilinear  $\gamma WW$  coupling and the diagram with quartic  $\gamma\gamma WW$  coupling.

stant at the asymptotic value  $\sigma \simeq 8\pi\alpha^2/M_W^2 \simeq 80$  pb and practically independent on photon polarization [8], see the formulas in Subsection II B. At  $\sqrt{s} > 200$  GeV this cross section is more than ten times larger than the cross section of  $W$  production in  $e^+e^-$  mode. It will ensure very high event rate at the anticipated luminosity. The distributions of  $W^+$  and  $W^-$  bosons in  $\gamma\gamma \rightarrow W^+W^-$  process are identical (charge symmetrical distribution), their polarizations are determined by the polarization of initial photons. The distribution of muons in subsequent decay of polarized  $W^\pm$  is asymmetrical due to P non-conservation with CP conservation in the SM.

### A. Diagrams

In this section we classify all tree level diagrams describing the process  $\gamma\gamma \rightarrow W^\pm\mu^\mp\nu$  and  $\gamma\gamma \rightarrow \mu^+\mu^-\nu\bar{\nu}$  in classes according to their topology (a similar classification was given also in Ref. [7]). For each topology we give an analytical estimate of its asymptotic contribution to the total cross section at  $s \gg M_W^2$ , identifying in each group the  $2 \rightarrow 2$  dominant subprocess and assuming for the SM gauge couplings  $g^2 \sim g'^2 \sim e^2 = 4\pi\alpha$ . The numerical Monte Carlo results, supporting these estimates, are presented in the next Sections.

The processes  $\gamma\gamma \rightarrow W^\pm\mu^\mp\nu$  are described by seven diagrams, which we divide in three classes, shown in Fig. 1:

- (a) Three double-resonant diagrams (DRD) of Fig. 1(a) describe  $WW$  pair production with subsequent decay. Their contribution to the total cross section is  $\sigma_d \sim \sigma_{\gamma\gamma \rightarrow WW} Br(W \rightarrow \mu\nu) \sim (\alpha^2/M_W^2) Br(W \rightarrow \mu\nu)$ .
- (b) Two single-resonant diagrams (SRDW) of Fig. 1(b) with  $W$  exchange in  $t$ -channel contribute to the total cross section  $\sigma_s \sim \alpha\sigma_{\gamma\gamma \rightarrow WW} \sim (\alpha^3/M_W^2)$ . The relation between this contribution and DRD contribution is  $\sigma_s/\sigma_d \sim \alpha/Br(W \rightarrow \mu\nu)$ .
- (c) Two single resonant diagrams (SRD $\mu$ ) with lepton exchange in  $t$ -channel (gauge boson

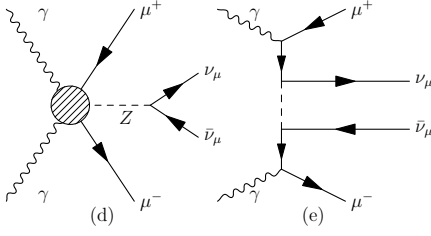


FIG. 2: Additional tree level Feynman diagrams contributing to  $\gamma\gamma \rightarrow \mu^+\mu^-\nu\bar{\nu}$ : the grey blob in (d) represents diagrams with  $\mu\mu$  fusion to  $Z$  and diagrams with  $Z$  radiated by an external  $\mu$  line.

bremsstrahlung), Fig. 1(c). The contribution to the total cross section is  $\sigma_{s\mu} \sim \alpha\sigma_{\gamma\gamma\rightarrow\mu\mu} \sim (\alpha^3/s)$ , therefore  $\sigma_{s\mu}/\sigma_d \sim [\alpha/Br(W \rightarrow \mu\nu)](M_W^2/s)$ .

The process  $\gamma\gamma \rightarrow \mu\mu\nu\bar{\nu}$  is described by the diagrams Fig. 1 with the addition of lines describing the  $W \rightarrow \mu\nu$

decay and permutations of external fermion lines (with the same estimates as above) and two additional types of diagrams shown in Fig. 2.

(d) Six diagrams with radiation of  $Z$  boson in the process  $\gamma\gamma \rightarrow \mu^+\mu^-$ , Fig. 1(d). The asymptotic contribution is  $\sigma_Z \sim \alpha\sigma_{\gamma\gamma\rightarrow\mu\mu}\alpha Br(Z \rightarrow \nu\bar{\nu}) \sim (\alpha^3/s)Br(Z \rightarrow \nu\bar{\nu})$ .

(e) Two multi-peripheral non-resonant diagrams Fig. 1(e) with  $\sigma_n \sim \alpha^4/M_W^2$ .

## B. Qualitative picture

The above analysis shows that the bulk of the cross section is given by the diagrams containing the process  $\gamma\gamma \rightarrow W^+W^-$  with subsequent decay of  $W$  bosons to leptons Fig. 1(a), DRD diagrams.

Denoting by  $p_\perp$   $W$ 's transverse momentum, the  $\gamma\gamma \rightarrow W^+W^-$  differential cross section can be written as [8]:

$$\begin{aligned} d\sigma &= d\sigma^{np} + \lambda_1\lambda_2 d\tau^a, \quad \sigma_W = \frac{8\pi\alpha^2}{M_W^2}, \quad x = \frac{4M_W^2}{s}, \quad dt = -dp_\perp^2 \sqrt{\frac{s}{s - 4(p_\perp^2 + M_W^2)}}, \\ d\sigma^{np} &= \sigma_W \left[ \frac{(16 + 3x^2)M_W^2}{32(p_\perp^2 + M_W^2)^2} - \frac{(3 + 8x)x}{32(p_\perp^2 + M_W^2)} + \frac{3x^2}{64M_W^2} \right] dt, \\ d\tau^a &= \sigma_W \left[ -\frac{xM_W^2}{2(p_\perp^2 + M_W^2)^2} + \frac{(3 + 8x)x}{32(p_\perp^2 + M_W^2)} - \frac{3x^2}{64M_W^2} \right] dt, \end{aligned} \quad (4)$$

with total cross section ( $v = \sqrt{1 - x}$ ),

$$\sigma = \sigma_W v \cdot \left\{ 1 + \frac{3x}{16} + \frac{3x^2}{16} - \left(1 - \frac{x}{2}\right) \frac{3x^2}{16v} \log \frac{1+v}{1-v} + \frac{x\lambda_1\lambda_2}{16} \cdot \left[ -19 + \frac{(8 - 5x)}{v} \log \frac{1+v}{1-v} \right] \right\}. \quad (5)$$

From the analysis of these equations we can see that at  $\sqrt{s} > 200$  GeV the  $\gamma\gamma \rightarrow W^+W^-$  differential cross section practically does not depend on photon polarizations, as for standard QED process, total cross section is practically energy independent, at the plateau value  $\sigma_W = 8\pi\alpha^2/M_W^2$ . Moreover, the  $W$ 's are produced mainly in the forward and backward directions, with average transverse momentum  $\sim M_W$  (distribution  $\propto 1/(p_\perp^2 + M_W^2)^2$ ).

As shown in Ref. [9], in this process we have an approximate helicity conservation. For  $p_\perp = 0$ , the helicity of  $W^\pm$  moving in the positive direction of  $z$  axis is  $\lambda_{W_1} = \lambda_1$ , irrespective of the charge of the  $W$ ; the same holds for the  $W$  moving in the opposite direction:  $\lambda_{W_2} = \lambda_2$ . These identities do not hold for  $p_\perp \neq 0$  and become less and less accurate with increasing values of  $p_\perp$ . Since in our process the cross section is concentrated at small values of  $p_\perp$ , we have an approximate helicity conservation:  $\lambda_{W_1} \approx \lambda_1$ , and  $\lambda_{W_2} \approx \lambda_2$ , both for  $W^+$

and  $W^-$ .

Now we can qualitatively understand the origin of charge asymmetries. Let  $z'$ -axis be directed along  $W$  three-momentum and  $\varepsilon \approx M_W/2$  and  $p_{z'}$  be the energy and the longitudinal momentum of  $\mu$  in the  $W$  rest frame. It is easy to calculate that the distribution of muons from the decay of  $W$  with charge  $e = \pm 1$  and helicity  $\lambda = \pm 1$  in its rest frame is  $\propto (\varepsilon - e\lambda p_{z'})^2$  (the transverse momenta of muons are distributed roughly isotropically relative to  $W$  momentum within the interval  $p_\perp < m_W/2$ ). In other words, the distribution of muons from  $W^\pm$  decay has a peak along  $W$  momentum if the  $e \cdot \lambda_W = -1$  and opposite to  $W$  momentum if  $e \cdot \lambda_W = +1$ . These distributions are boosted to the distributions in the  $\gamma\gamma$  collision frame. For example, for a collision of photons in a  $\gamma_-\gamma_-$  initial state, the  $\mu^-$  are distributed around the upper value of their longitudinal momentum (in forward and backward direction), while the  $\mu^+$  are concentrated near the zero value of their longitudinal momentum. At the same time,

this boost makes the distribution in  $p_\perp$  wider in the first case and narrower in the second case.

### C. Cuts

It is natural to expect that the relative size of New Physics effects will be enhanced with the growth of transverse momenta of observed particles. This is the main reason why we study the dependence of observed effects on the cut in  $p_\perp$ . Namely, we impose cuts on the transverse momenta of observed charged particles,  $p_{\perp\mu}^c$  and on the scattering angle

$$p_\perp > p_{\perp\mu}^c, \quad \theta_0 < \theta < \pi - \theta_0, \quad \theta_0 = p_{\perp\mu}^c / 2E. \quad (6)$$

The cut (6) is applied to each observed particle and to the total transverse momentum for the sum of momenta of all observed particles; the cut for escape angle is applied to all the observed particles. We consider the dependence of all studied quantities on the  $p_{\perp\mu}^c$  up to  $p_{\perp\mu}^c = 140$  GeV. This cut also mimics limitations from the detector in the future experiment.

These simultaneous cuts allow to eliminate many backgrounds (since charged particle(s) with missing transverse momentum greater than  $p_{\perp\mu}^c$  should have the escape angle greater than  $2p_{\perp\mu}^c / \sqrt{s} > \theta_0$ ). In particular, all pure QED and QCD processes are eliminated by these cuts, since they cannot provide large missing transverse momentum.

If it is not otherwise specified, in the following we set  $p_{\perp\mu}^c = 10$  GeV,  $\theta_0 = 20$  mrad, and monochromatic photon beams at  $\sqrt{s}_{\gamma\gamma} = 500$  GeV ( $E_\gamma = 250$  GeV).

The effect of cuts with non-monochromatic photons is studied in sect. VI.

### D. Variables for description of global asymmetry

The global asymmetry variables are described by the difference in distributions of  $\mu^+$  and  $\mu^-$  in the processes  $\gamma\gamma \rightarrow W^+\mu^- + \nu$ 's and  $\gamma\gamma \rightarrow W^-\mu^+ + \nu$ 's (or in  $\gamma\gamma \rightarrow \mu^+\mu^- + \nu$ 's). For definiteness, we calculate all quantities only for the case when negatively charged particle ( $W^-$  or  $\mu^-$ ) is in the forward hemisphere ( $p_\parallel > 0$ ). In the study of the dependence on  $p_{\perp\mu}^c$ , we will label all the quantities by the argument ( $p_{\perp\mu}^c$ ).

A suitable measure for the *longitudinal* ( $\Delta_L$ ) and *transverse* ( $\Delta_T$ ) charge asymmetries are the relative differences of corresponding momenta distributions for negative and positive muons:

$$\Delta_L = \frac{\int p_\parallel^- d\sigma - \int p_\parallel^+ d\sigma}{\int p_\parallel^- d\sigma + \int p_\parallel^+ d\sigma}, \quad \Delta_T = \frac{\int p_\perp^- d\sigma - \int p_\perp^+ d\sigma}{\int p_\perp^- d\sigma + \int p_\perp^+ d\sigma}. \quad (7)$$

It is useful to define also mean values of longitudinal  $p_\parallel^\mp$  and transverse  $p_\perp^\mp$  momenta of  $\mu^-$  or  $\mu^+$

$$P_L^\pm = \frac{\int p_\parallel^\pm d\sigma}{E_{\gamma max} \int d\sigma}, \quad P_T^\pm = \frac{\int p_\perp^\pm d\sigma}{E_{\gamma max} \int d\sigma}. \quad (8)$$

(These definitions are written in the form which is useful for non-monochromatic case as well.)

Due to CP symmetry of the SM,

$$\begin{aligned} d\sigma_{--}(p_{\mu^+}, p_{\mu^-}) &= d\sigma_{++}(p_{\mu^-}, p_{\mu^+}) \\ d\sigma_{+-}(p_{\mu^+}, p_{\mu^-}) &= d\sigma_{-+}(p_{\mu^-}, p_{\mu^+}). \end{aligned} \quad (9)$$

(Here subscripts  $+$  and  $-$  at cross section label initial photon helicities).<sup>1</sup> In particular, the distributions of  $\mu^-$  and  $\mu^+$  in the forward hemisphere for  $\gamma_+\gamma_-$  collision reproduce the distributions of  $\mu^+$  and  $\mu^-$  in the backward hemisphere. Therefore, in all the cases the asymmetries  $\Delta_L$  (determined by Eq. (7)) change signs in each hemisphere when the helicity changes to opposite. For the  $\gamma_-\gamma_+$  collisions these asymmetries in forward and backward hemispheres have opposite signs. These symmetries break if any CP-violating interaction is present.

Total cross sections of the processes  $\gamma\gamma \rightarrow W^+\mu^- + \nu$ 's and  $\gamma\gamma \rightarrow W^-\mu^+ + \nu$ 's coincide at each initial photon polarization. However, in accordance with above discussed qualitative picture, applied cuts reduce these cross section in different way. So that, it is useful to define relative value of this difference in dependence on cut variable,

$$\Delta\sigma(p_{\perp\mu}^c) = \frac{(\int d\sigma(W^-\mu^+) - \int d\sigma(W^+\mu^-))_{(p_\perp > p_{\perp\mu}^c)}}{(\int d\sigma(W^-\mu^+) + \int d\sigma(W^+\mu^-))_{(p_\perp > p_{\perp\mu}^c)}}, \quad (11)$$

and the fraction of the total cross section left by the cut in  $p_{\perp\mu}^c$ :

$$\sigma^\pm(p_{\perp\mu}^c) = \int d\sigma(W^\mp \mu^\pm)_{(p_\perp > p_{\perp\mu}^c)}. \quad (12)$$

### E. Estimate of statistical uncertainties

MC calculations simulate an experiment and have some statistical uncertainty  $\delta_{MC}$ . This uncertainty value

<sup>1</sup> One can write the differential distribution in the reaction  $\gamma\gamma \rightarrow \mu^+\mu^- + \nu$ 's as

$$\frac{d\sigma}{d^3p_{\mu^+} d^3p_{\mu^-}} = A + B\lambda_1 + C\lambda_2 + D\lambda_1\lambda_2 \quad (10)$$

That is another form of eq. (9) with  $\int Bd^3p_{\mu^+} d^3p_{\mu^-} = 0$ ,  $\int Cd^3p_{\mu^+} d^3p_{\mu^-} = 0$ . The weak dependence of the cross section on the photon polarization means that  $\int Dd^3p_{\mu^+} d^3p_{\mu^-} \ll \int Ad^3p_{\mu^+} d^3p_{\mu^-}$ . Our subsequent analysis based on momentum distributions shows that on average  $|D| \sim |B| \sim |C| \sim |A|$ . In the following paragraphs and sections we will not make use of the form in Eq. (10).

for the integral characteristics like (7) cannot be predicted simply from general reasons. To find this uncertainty we repeated our MC calculation with anticipated  $10^6$  number of events five times for different random number inputs for MC generator. Additionally we consider as an independent input the set of observations obtained by simultaneous change  $\lambda_1, \lambda_2 \rightarrow -\lambda_1, -\lambda_2$ ,  $\mu^- \leftrightarrow \mu^+$  (this change should not change distributions due to CP conservation in SM), in whole it corresponds ten repetitions of "MC experiment" in a sum. These sets of data were an input for standard generation of Monte Carlo inaccuracies  $\delta_{MC}$ .

Since the adaptive MC is used with CalcHEP, it is natural to expect that the statistical uncertainty of future real experiment  $\delta_{exp}^{stat} \geq \delta_{MC}$ . Therefore, below we omit subscript MC, having in mind that our numbers give estimate for statistical uncertainty from below.

### III. GLOBAL ASYMMETRIES IN THE MAIN PROCESS $\gamma\gamma \rightarrow W^\pm \mu^\mp \nu$ . MONOCHROMATIC CASE

We start with the study of asymmetry neglecting the cascade channel and supposing photon beams monochromatic and completely polarized. First, we present the distributions  $\partial^2\sigma/(\partial p_\parallel \partial p_\perp)$  of muons in the  $(p_\parallel, p_\perp)$  plane, at different photon polarizations, in Figs. 3. These figures show explicitly strong difference in the distributions of negative and positive muons as well as strong dependence of distributions on photon polarizations. Therefore, the charge asymmetry in the process is a *strong effect*.

Table I presents obtained average momenta for the negative and positive muons and corresponding asymmetry quantities (7) together with their statistical uncertainties

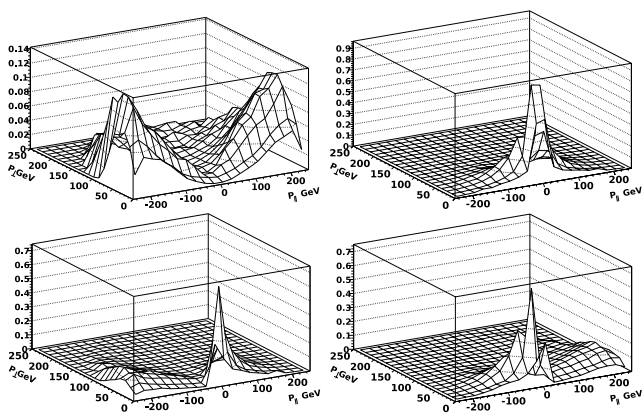


FIG. 3: Muon distribution in  $\gamma-\gamma \rightarrow W\mu\nu$  (upper plots) and in  $\gamma+\gamma- \rightarrow W\mu\nu$  (lower plots), left column  $\mu^-$ , right column  $\mu^+$ .

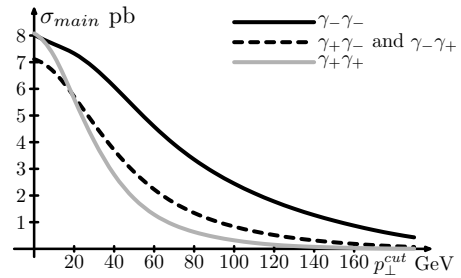


FIG. 4: Dependence of cross sections on cut  $p_{\perp\mu}^c$  for main process.

(in percents) for different cuts  $p_{\perp\mu}^c$ . One can see that the values of asymmetry are typically 20-50%.

We have checked that with the change of sign of both photon helicities mean muon momenta for negative and positive muons change their places (within statistical accuracy) so that the quantities  $\Delta_{L,T}$  change their signs with this change of polarization.

The longitudinal scale of distributions in momenta is determined by initial photon energy while the transverse scale is determined by the  $W$  mass. Hereupon mean transverse momenta are usually smaller than longitudinal.

Besides, for the collision of photons with identical helicity at the growth of cut  $p_{\perp\mu}^c$  the cross sections for production of positive and negative muons become different, due to discussed charge asymmetry (remind, we discuss only events with negative muons or  $W$ 's flying in forward hemisphere). For the collision of photons with opposite helicity these cross sections should coincide since, for example, for  $\gamma-\gamma+$  collision forward hemisphere for  $\mu^-$  production realize absolutely the same distribution as backward hemisphere for  $\mu^+$  production. This effect is clearly seen from Figure 4, where we present the  $p_{\perp\mu}^c$

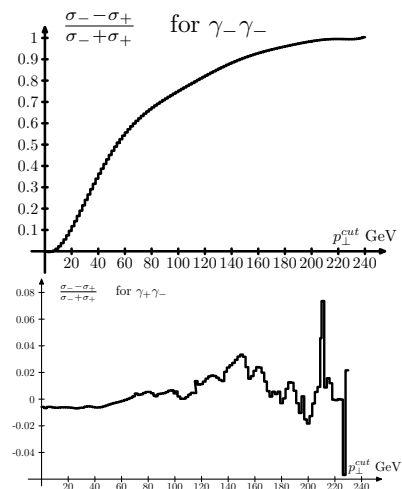


FIG. 5: Relative cross section differences in dependence on cut  $p_{\perp\mu}^c$  value.

| $p_{\perp\mu}^c$ | $\gamma_{\lambda_1}\gamma_{\lambda_2}$ | $P_L^-$ | $\delta P_L^-$ | $P_L^+$ | $\delta P_L^+$ | $\Delta_L$ | $\delta\Delta_L$ | $P_T^-$ | $\delta P_T^-$ | $P_T^+$ | $\delta P_T^+$ | $\Delta_T$ | $\delta\Delta_T$ |
|------------------|--|---------|----------------|---------|----------------|------------|------------------|---------|----------------|---------|----------------|------------|------------------|
| 10               | $\gamma_-\gamma_-$                     | 0.606   | 0.29%          | 0.201   | 0.55 %         | +0.501     | 0.57%            | 0.333   | 0.61%          | 0.159   | 0.28%          | +0.355     | 0.44%            |
|                  | $\gamma_+\gamma_-$                     | 0.223   | 0.74%          | 0.609   | 0.19 %         | -0.463     | 0.47%            | 0.164   | 0.08%          | 0.262   | 0.31%          | -0.231     | 0.76%            |
| 40               | $\gamma_-\gamma_-$                     | 0.593   | 0.39%          | 0.273   | 0.20 %         | +0.370     | 0.47%            | 0.378   | 0.64%          | 0.241   | 0.62%          | +0.222     | 1.07%            |
|                  | $\gamma_+\gamma_-$                     | 0.296   | 0.64%          | 0.637   | 0.25 %         | -0.366     | 0.66%            | 0.239   | 0.28%          | 0.319   | 0.25%          | -0.143     | 0.31%            |
| 140              | $\gamma_-\gamma_-$                     | 0.402   | 0.68%          | 0.242   | 0.14 %         | +0.249     | 1.45%            | 0.697   | 0.11%          | 0.621   | 0.04%          | +0.057     | 0.95%            |
|                  | $\gamma_+\gamma_-$                     | 0.253   | 0.81%          | 0.489   | 0.27 %         | -0.318     | 1.33%            | 0.672   | 0.12%          | 0.660   | 0.05%          | -0.009     | 5.75%            |

TABLE I: Charge asymmetry quantities and their statistical uncertainties for the process  $\gamma_{\lambda_1}\gamma_{\lambda_2} \rightarrow W\mu\nu$ .

dependence for cross sections (12) at different initial photon polarizations.

The corresponding cross section differences, Eq. (11), are shown in Figure 5 *without averaging over realizations*. The difference in cross sections for  $\gamma_-\gamma_-$  and  $\gamma_+\gamma_+$  collisions is due to our choice of events with negative particles in forward hemisphere. In this case the cross sections coincide at small  $p_{\perp\mu}^c$ , while at high  $p_{\perp\mu}^c$  one of them becomes larger and larger in comparison with the other, thus  $\Delta\sigma$  goes to one (one more demonstration of transverse asymmetry). For the case with opposite photon helicities the deviation of  $\Delta\sigma$  from zero shows high statistical uncertainty, due to the very low value of the cross sections (low counting rates) at  $p_{\perp\mu} > 120$  GeV. Similar dependencies with roughly the same characteristic values of  $p_{\perp\mu}^c$  remain valid even at higher collision energies (for example, at  $\sqrt{s} = 2$  TeV) since the scale of this dependence is determined by the  $W$  boson mass and not by the total energy.

#### IV. GLOBAL ASYMMETRIES IN CASCADE PROCESS WITH INTERMEDIATE $\tau$

The observable final state with two muons or  $W + \mu$  with missing transverse momentum carried away by neutrinos can appear either via processes  $\gamma\gamma \rightarrow \mu^+\mu^-\nu_\mu\bar{\nu}_\mu$  ( $\gamma\gamma \rightarrow W\mu\nu$ ) or via cascade processes with  $\tau$  production and subsequent  $\tau$  decay ( $\tau \rightarrow \mu\nu_\mu\nu_\tau$ ), see Eq.(3). The latter process enhances the total event rate (without cuts) by a value given by factor  $B \equiv Br(\tau \rightarrow \mu\nu\nu) = 17\%$  for the  $\gamma\gamma \rightarrow W\mu + \nu's$ . Similar event rate enhancement in the process  $\gamma\gamma \rightarrow \mu^+\mu^- + \nu's$  is  $2B + B^2 \approx 37\%$ .

The accurate calculation of processes with six or more particles in the final state like  $\gamma\gamma \rightarrow \mu^+\mu^-\nu_\mu\bar{\nu}_\mu\nu_\tau\bar{\nu}_\tau$  is a computationally challenging task with available software. Since  $\tau$  is very narrow particle, the diagrams without  $\tau$ -pole in  $s$ -channel can be neglected with very high precision, ( $\sim \Gamma_\tau/m_\tau$ ). Therefore, one can in principle use the results for  $\gamma\gamma \rightarrow W\tau\nu$  ( $\gamma\gamma \rightarrow \tau^+\mu^-\nu_\mu\bar{\nu}_\mu$ , etc.) and convolute them with the distribution of  $\mu$  from  $\tau$  decay. However, the latter distribution depends on  $\tau$  polarization which cannot be determined definitely with CompHEP/CalcHEP in general case. (Generally, all helicity amplitudes for  $\tau$  production are nonzero, and for convolution one must

consider not only diagonal helicity states but also their interference).

Fortunately, the cascade process provides only a small fraction of the total cross section and the main contribution to the total cross section is given by the double resonant (DRD) diagrams of Fig. 1(a). That is the reason why in the description of the cascade contribution only these diagrams can be taken into account — *DRD approximation*. In this approximation the  $\tau$  helicity is precisely determined in each MC event. In sect. V A we will show that the inaccuracy introduced in the total result using the DRD approximation for the cascade contribution is within the estimated statistical uncertainty, found for the main process.

Note that the distributions obtained in sect. III describe with high accuracy also  $\tau$ -distributions in  $\gamma\gamma \rightarrow W\tau\nu$  processes etc.

In the DRD approximation each  $\tau$  is produced only via  $W$ -decay, and its polarization in the rest frame of  $W$  is given by the SM vertex,  $\tau^+W_\mu^-\gamma^\mu(1-\gamma^5)\nu_\tau + h.c.$ . Due to  $\gamma^\mu(1-\gamma^5)$  factor,  $\tau$  helicity is opposite to that of  $\nu_\tau$ , it is positive for  $\tau^+$  and negative for  $\tau^-$  (with accuracy to  $m_\tau/M_W$ ) and independent on  $W$  polarization.

For each generated event momenta of all particles are known. The spin vector of  $\tau$  is expressed easily via momenta of  $\tau$  and  $\nu_\tau$ ,  $p_\tau$  and  $p_\nu$  respectively, as

$$\pm s/2, \text{ where } s = \left( \frac{p_\tau}{m_\tau} - \frac{p_\nu m_\tau}{(p_\tau p_\nu)} \right) \begin{cases} + & \text{for } \tau^+, \\ - & \text{for } \tau^-. \end{cases} \quad (13)$$

Denoting the momentum of  $\mu$  by  $k$ , the distribution of muons in  $\tau$ -decay with momentum  $p_\tau$  and spin  $\pm s$  can be written, neglecting muon mass, as

$$f = \frac{4}{\pi E_\tau m_\tau^5} [(3m_\tau^2 - 4p_\tau k)p_\tau k + ks \cdot m_\tau(4p_\tau k - m_\tau^2)] d\Gamma, \quad (14)$$

where  $d\Gamma$  is a phase space element boosted to the lab frame. In the  $\tau$  rest frame  $d\Gamma = \theta(m_\tau/2 - k)d^3k/E_\mu$ . Note that the sign of helicity before  $s$  in Eq. (13) disappears in the result.

Let us discuss now the qualitative features of the muon spectrum given by the convolution of the  $\tau$  spectrum with the distribution in Eq. (14). One can consider  $\tau \rightarrow \mu\nu\nu$  decay as a two body decay: a massless muon and the di-neutrino with invariant mass  $m_{\nu\nu}$ . At given  $m_{\nu\nu}$ , the

energy and 3-momentum of the muon in the  $\tau$  rest frame are  $\varepsilon_\mu = p_\mu^0 = Am_\tau/2$  with  $A = 1 - (m_{\nu\nu}/m_\tau)^2$ . In the laboratory frame where the 3-momentum of the  $\tau$ ,  $\vec{p}_\tau$  is under some angle  $\theta$  relative to muon momentum in  $\tau$  rest frame, the muon momentum is evidently  $\vec{p}_\mu = A\vec{p}_\tau(1 + \cos\theta)/2$  plus small corrections negligible in our discussion. Therefore, the muon distribution repeats in some sense that of the  $\tau$  but with a factor  $A(1 + \cos\theta)/2$ , which is usually much lower than one. In other words, the distribution of muons in the cascade process is similar in the main features to that of the  $\tau$  but it is *strongly contracted to the origin of the coordinates*.

- It is useful to describe the inaccuracy of the DRD approximation in the description of the  $\gamma\gamma \rightarrow W\tau\nu$  cross section itself,  $\delta_{DRD}^{\tau W}$ , in dependence on the cut  $p_{\perp\tau}^c$ . The estimates in Sec. II A show that at the considered energies all contributions to the cross section are small in comparison with that of the DRD except for the SRDW contribution. The interference term  $Re(A_{DRD}^* A_{SRDW})$  is roughly of the same order of magnitude as  $|A_{SRDW}|^2$  since the DRD is large only in regions of the final phase space corresponding to the  $W$  resonances, while the other contributions do not have these peaks. The numerical value of this inaccuracy is obtained by direct comparison of this cross section, calculated with all diagrams, and those for DRD diagrams with MC simulation.

At  $p_{\perp\tau}^c = 10$  GeV we find that for the  $\gamma\gamma \rightarrow W\tau\nu$  process the SRDW contribution itself is about 5 % of the DRD one, and the interference of this contribution with DRD is destructive so that the DRD contribution differs from total cross section only by about 1%. This difference naturally grows with increasing values of  $p_{\perp\tau}^c$ .

More important for us is the inaccuracy of DRD approximation in the description of asymmetry quantities (7). Table II presents value of inaccuracy  $\delta_{DRD}^{\tau W}(p_{\perp\tau}^c)$  introduced by DRD approximation in the description of  $\gamma\gamma \rightarrow W\tau\nu$  process at different cut values of  $\tau$  *transverse momenta*  $p_{\perp\tau}^c$ .

| $p_{\perp\tau}^c$ , (GeV) | $\delta_L^{(-)}(\%)$ | $\delta_T^{(-)}(\%)$ | $\delta_L^{(+)}(\%)$ | $\delta_T^{(+)}(\%)$ |
|---------------------------|----------------------|----------------------|----------------------|----------------------|
| 10                        | 0.9                  | 2.3                  | 0.7                  | 3.45                 |
| 40                        | 1.5                  | 3.6                  | 2.1                  | 4.1                  |
| 80                        | 1.9                  | 5.6                  | 4.2                  | 7.7                  |
| 120                       | 5.7                  | 5.3                  | 4.4                  | 31                   |

TABLE II: Inaccuracy of DRD approximation  $\delta_{DRD}^{\tau W}(p_{\perp\tau}^c)$  for  $\Delta_{L,T}$  at different  $p_{\perp\tau}^c$  for  $\tau$  production.

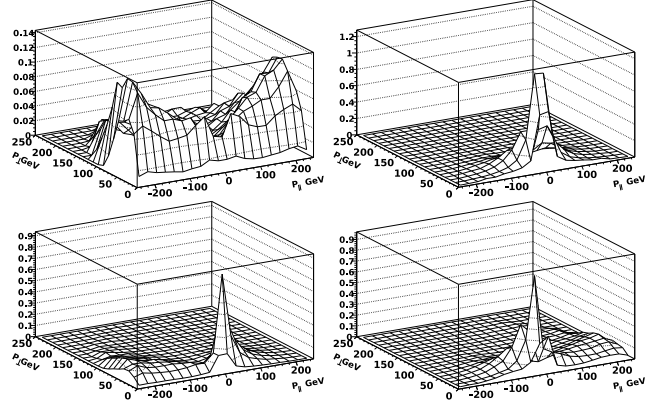


FIG. 7: Total muon distribution in  $\gamma\gamma \rightarrow W\mu + \nu's$  (upper plot) and  $\gamma\gamma \rightarrow W\mu + \nu's$  (lower plot); left -  $\mu^-$ , right -  $\mu^+$

Large values of the relative quantity  $\delta_T^{(+-)}$  at large  $p_{\perp\tau}^c$  appear in the case when the absolute value of  $\Delta_T^{(+-)}$  is negligibly small. One can see that this inaccuracy grows with increasing the value of the cut, see Fig. 5. However with this increase also the fraction of cascade process within the total process becomes smaller and smaller (see discussion at the end of next section).

For the processes  $\gamma\gamma \rightarrow \mu^\pm \tau^\mp \nu\nu$  and  $\gamma\gamma \rightarrow \tau^+ \tau^- \nu\nu$  the inaccuracies of DRD approximation are  $\delta_{DRD}^{\tau\mu}(p_{\perp\tau}^c) = \delta_{DRD}^{\tau W}(p_{\perp\tau}^c)$  and  $\delta_{DRD}^{\tau\tau}(p_{\perp\tau}^c) = 2\delta_{DRD}^{\tau W}(p_{\perp\tau}^c)$ .

## V. TOTAL ASYMMETRIES

The resulting distributions include the complete tree-level results of  $\gamma\gamma \rightarrow W\mu\nu$  and DRD approximation for cascade contribution.

Figures 7 show the total observable distributions of muons, i.e. the sum of distributions of muons in  $\gamma\gamma \rightarrow W\mu\nu$  and  $\gamma\gamma \rightarrow W\tau\nu \rightarrow W\mu\nu\nu$ , and Table III presents the corresponding total asymmetry quantities for  $p_{\perp\mu}^c = 10$  GeV. Comparison with Fig. 3 and Table I shows that the cascade process introduces a change in the shape of muons distribution only at small momenta and its contribution reduces the asymmetry parameters  $\Delta_{L,T}$  in average by about 3 % only.

The plots in Fig. 8 show the dependence of asymmetries  $\Delta_L$  and  $\Delta_T$  on  $p_{\perp\mu}^c$ . The longitudinal charge asym-

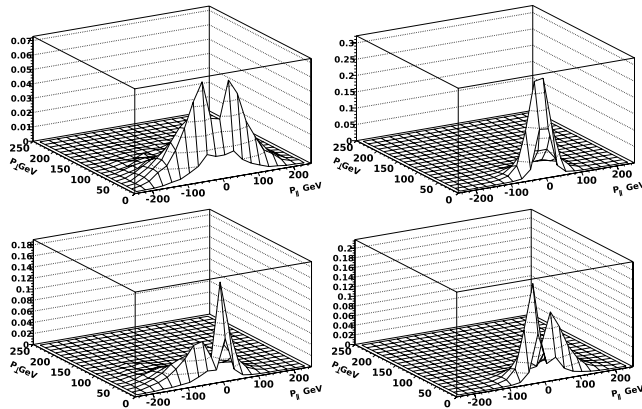


FIG. 6: Muon distribution in cascade processes  $\gamma\gamma \rightarrow W\mu\nu\nu\nu$  (upper plot) and  $\gamma\gamma \rightarrow W\mu\nu\nu\nu$  (lower plot), left -  $\mu^-$ , right -  $\mu^+$

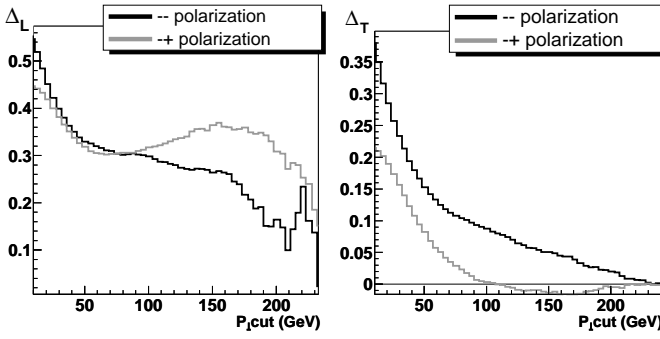


FIG. 8: The  $p_{\perp\mu}^c$  dependence of asymmetry. Left plot –  $\Delta_L$ , right plot –  $\Delta_T$ , black lines – for  $\gamma_-\gamma_-$ , gray lines – for  $\gamma_-\gamma_+$

metry remains large even with large cuts, while the transverse charge asymmetry diminishes with  $p_{\perp\mu}^c$  growth. In particular, for  $\gamma_+\gamma_-$  collision at  $p_{\perp\mu}^c \geq 120$  GeV the quantities  $P_T^+$  and  $P_T^-$  practically coincide, giving negligible  $\Delta_T$ , right plot, with naturally high statistical uncertainty in this small quantity.

The  $p_{\perp\mu}^c$  dependence of resulting cross sections for different photon polarizations is shown in Fig. 9. The difference in curves for  $(++)$  and  $(--)$  initial states arise because of our *charge asymmetric* selection of events, with negative particles flying in the forward hemisphere (see Sec. II D).

#### A. Inaccuracy of DRD approximation for resulting asymmetries

Let us denote by  $\delta_{DRD}^{tot}(p_{\perp\mu}^c)$  the inaccuracy of the DRD approximation for the resulting asymmetries, by  $\delta^{casc}(p_{\perp\mu}^c)$  — the inaccuracy of DRD approximation for the description of the cascade process itself, like that given in the Table II, and by

$$R(p_{\perp\mu}^c) = \frac{\sigma^{casc}(p_{\perp\mu}^c)}{\sigma^{tot}(p_{\perp\mu}^c)} \quad (15)$$

the relative contribution of cascade  $\mu$  in the total cross section, all – in dependence on cut for muons  $p_{\perp\mu}^c$ . Naturally,

$$\delta_{DRD}^{tot}(p_{\perp\mu}^c) = R(p_{\perp\mu}^c) \delta^{casc}(p_{\perp\mu}^c). \quad (16)$$

Due to the contraction of the distribution of muons produced in the cascade process in comparison with that

| $\gamma_{\lambda_1}\gamma_{\lambda_2}$ | $P_L^-$ | $P_L^+$ | $\Delta_L$ | $P_T^-$ | $P_T^+$ | $\Delta_T$ |
|--|---------|---------|------------|---------|---------|------------|
| $\gamma_-\gamma_-$                     | 0.548   | 0.164   | +0.539     | 0.311   | 0.142   | +0.374     |
| $\gamma_+\gamma_-$                     | 0.199   | 0.513   | -0.440     | 0.152   | 0.232   | -0.207     |

TABLE III: Resulting asymmetry quantities.

of the parental  $\tau$  (see Sec. IV), and consequently with that of  $\mu$  in the main process, the relative contribution of the cascade  $\mu$  in the total cross section  $R(p_{\perp\mu}^c)$  falls rapidly with the growth of the cut  $p_{\perp\mu}^c$ , as can be seen in Fig. 10.

At  $p_{\perp\mu}^c = 0$  we have  $\delta^{casc}(p_{\perp\mu}^c) = \delta^{casc}(p_{\perp\tau}^c)$ . With the numbers given by Table II and Fig. 10 one can see that the inaccuracies (16) are lower than the expected statistical uncertainty of future experiments (Table I, first two lines). With growth of  $p_{\perp\mu}^c$  the inaccuracy  $\delta^{casc}(p_{\perp\mu}^c)$ , similar to that given in the Table II, increases, but the cascade contribution  $R(p_{\perp\mu}^c)$ , Fig. 10, decreases faster. Therefore the resulting inaccuracy introduced by the DRD approximation in Eq. (16) is well within the expected statistical uncertainty of future experiments, Table I, at each cut on transverse momentum for the  $\gamma\gamma \rightarrow W\mu + \nu's$  process (and it is within the expected statistical uncertainty of future experiments for  $\gamma\gamma \rightarrow \mu^+\mu^- + \nu's$  process).

#### VI. EFFECT OF PHOTON NON-MONOCROMATICITY

At the PC photons will be non-monochromatic with spectra peaked near the high energy limit  $E_{\gamma}^{max}$ . Moreover, due to the finite distance between the conversion point (CP) and the interaction point (IP) and also due to rescatterings of laser photons on electrons after the first collision, photon spectra are even non-factorizable. Fortunately in their high energy part, ( $E_{\gamma} > E_{\gamma}^{max}/\sqrt{2}$ ), these spectra are factorizable with a high precision and these photons have a high degree of polarization. Moreover, the form of the effective spectra in this region is described with high accuracy with the aid of only one additional parameter, independent from the details of the experimental setup, while the polarization is the same as for pure Compton effect [10]. *The luminosity of the Photon Collider is normalized for this very region only.*

The low energy part of the effective photon spectrum, depends strongly on the details of the experimental setup which may change during the construction process of the

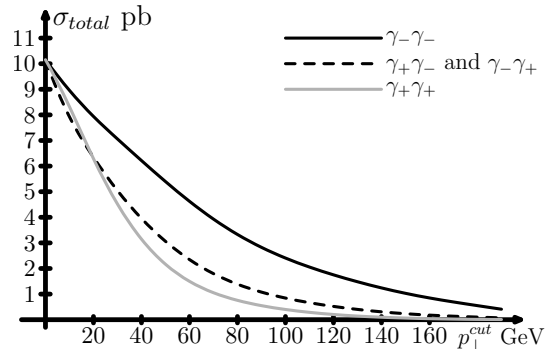


FIG. 9: The  $p_{\perp\mu}^c$  dependence of resulting cross sections for different photon polarizations.



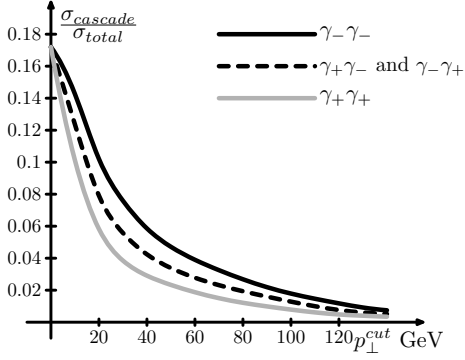


FIG. 10: Relative contribution of the cascade process  $R(p_{\perp\mu}^c)$  as defined in Eq.15 vs  $p_{\perp\mu}^c$ .

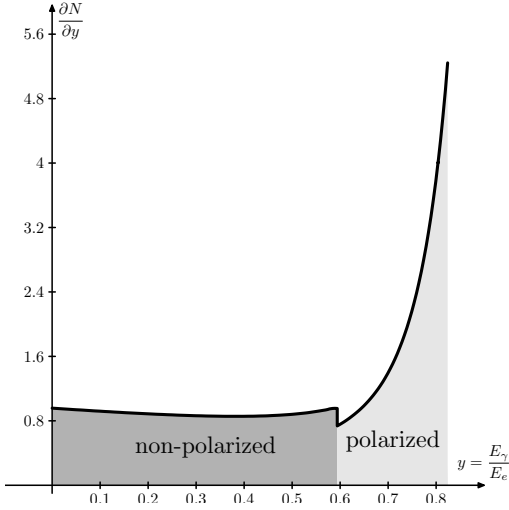


FIG. 11: The "realistic" photon spectra, used in our calculations.

ILC. Therefore, in our simulations, we used a photon spectrum composed of two parts as shown in Fig. 11. At  $E_\gamma > E_\gamma^{max}/\sqrt{2}$  we used the approximation from Ref. [10] with  $\rho = 1$  and  $x = 4.8$  with polarization for ideal Compton effect [2]. In order to imitate the low energy part of the spectrum (at  $E_\gamma < E_\gamma^{max}/\sqrt{2}$ ) we used spectra from [2] for the case when the IP and CP coincide ( $\rho = 0$ ) and consider these photons to be unpolarized.

In this section we denote by  $\gamma_-$  an initial photon state obtained in collision of laser photon with helicity  $P_c = +1$  and an electron with mean double initial helicity  $2\lambda_e = 0.85$ , which gives  $\lambda_\gamma = -1$  for photons with  $E_\gamma = E_\gamma^{max}$ . In this case mean polarization of photons with  $E_\gamma > E_\gamma^{max}/\sqrt{2}$  is also negative but its absolute value is lower than one as it is described in [2]. At  $E_\gamma < E_\gamma^{max}/\sqrt{2}$  we treat these photons as non-polarized. The state  $\gamma_+$  is defined in the same way.

The resulting distributions of muons are presented on Fig. 12 for the case when incident electron energies are 250 GeV and the laser parameter is  $x = 4.8$ . They re-

semble those presented in Fig. 3 with additional maximum at low energies. Table IV shows the corresponding asymmetry quantities. These values are slightly smaller in comparison to the monochromatic case, but they are still large enough and replicate in main features the values in Table I with approximately the same statistical uncertainties.

## VII. CORRELATIVE ASYMMETRIES IN $\gamma\gamma \rightarrow \mu^+\mu^- + \nu'S$

The charge asymmetry in relative distributions of positive and negative muons in each event can be a more useful instrument to hunt for the New Physics (but with lower counting rates). A simple analogy in terms of charge symmetric variables, is provided by transverse momentum and invariant mass distribution. The global asymmetry distribution corresponds to that in transverse momentum while the correlative asymmetry distribution corresponds to that in the effective  $\mu^+\mu^-$  mass. The latter is sensitive to the existence of possible resonance states, which cannot be seen in global asymmetries. As an example we present distribution in  $\vec{k} = \vec{p}_+ + \vec{p}_-$  in its longitudinal and transverse component, Fig. 13.

In the case of charge symmetry this distribution would be centered around the point  $(k_{\parallel}, k_{\perp}) = (0, 0)$ . This figure exhibits strong effect of charge asymmetry.

The first problem for numerical analysis here is to find some representative variables in 5-dimensional space of observables  $\vec{p}_+ \vec{p}_-$ . We consider three representative "natural" dimensionless variables for  $\gamma\gamma \rightarrow \mu^+\mu^- \nu\bar{\nu}$  process:

$$\begin{aligned} v &= \frac{4(p_{\perp+}^2 - p_{\perp-}^2)}{M_W^2}, & u &= \frac{4(p_{\parallel+}^2 - p_{\parallel-}^2)}{M_W^2}, \\ w &= \frac{4(p_{\parallel+}\epsilon_+ - p_{\parallel-}\epsilon_-)}{M_W^2}, \end{aligned} \quad (17)$$

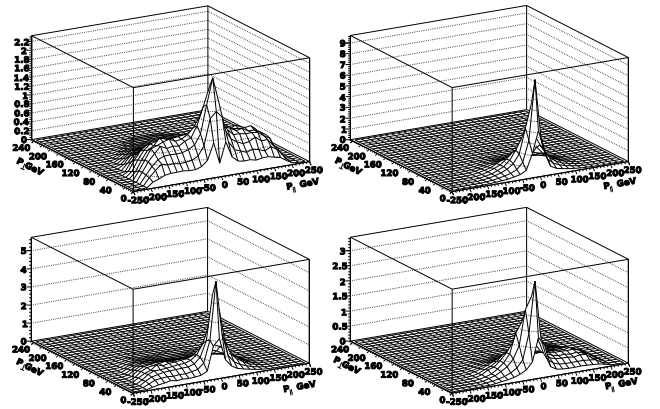


FIG. 12: The distributions of muons calculated with "realistic" spectra distribution. Upper plots -  $\gamma-\gamma-$ . Lower plots -  $\gamma+\gamma-$ . Left -  $\mu^-$ , right -  $\mu^+$

| $p_{\perp\mu}^c$ | $\gamma_{\lambda_1\gamma_{\lambda_2}}$ | $P_L^-$ | $\delta P_L^-$ | $P_L^+$ | $\delta P_L^+$ | $\Delta_L$ | $\delta\Delta_L$ | $P_T^-$ | $\delta P_T^-$ | $P_T^+$ | $\delta P_T^+$ | $\Delta_T$ | $\delta\Delta_T$ |
|------------------|--|---------|----------------|---------|----------------|------------|------------------|---------|----------------|---------|----------------|------------|------------------|
| 10               | $\gamma_-\gamma_-$                     | 0.365   | 0.31%          | 0.157   | 0.22%          | +0.398     | 0.18%            | 0.284   | 0.38%          | 0.179   | 0.10%          | +0.228     | 0.81%            |
|                  | $\gamma_+\gamma_-$                     | 0.174   | 0.24%          | 0.338   | 0.08%          | -0.321     | 0.43%            | 0.200   | 0.09%          | 0.236   | 0.16%          | -0.082     | 0.42%            |
| 40               | $\gamma_-\gamma_-$                     | 0.375   | 0.52%          | 0.199   | 0.16%          | +0.308     | 0.65%            | 0.352   | 0.15%          | 0.268   | 0.14%          | +0.136     | 0.51%            |
|                  | $\gamma_+\gamma_-$                     | 0.204   | 0.51%          | 0.386   | 0.13%          | -0.308     | 0.56%            | 0.278   | 0.14%          | 0.319   | 0.13%          | -0.067     | 0.82%            |
| 80               | $\gamma_-\gamma_-$                     | 0.355   | 0.47%          | 0.208   | 0.23%          | +0.263     | 0.88%            | 0.515   | 0.08%          | 0.449   | 0.06%          | +0.069     | 0.53%            |
|                  | $\gamma_+\gamma_-$                     | 0.207   | 0.38%          | 0.338   | 0.17%          | -0.305     | 0.75%            | 0.467   | 0.06%          | 0.483   | 0.03%          | -0.017     | 2.53%            |

TABLE IV: Charge asymmetry quantities for "realistic" photon spectra,  $\sqrt{s_{ee}} = 500$  GeV.

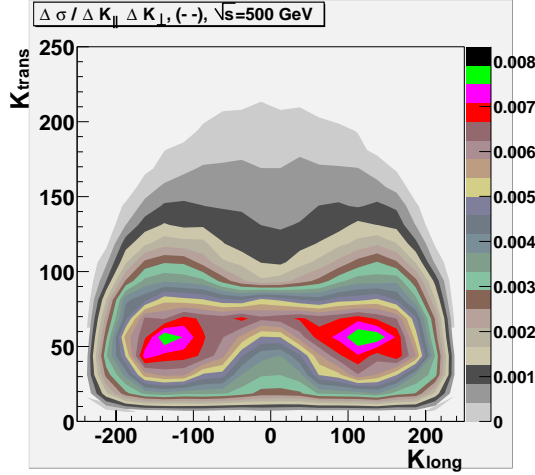


FIG. 13: Distribution in  $k_{\parallel}, k_{\perp}$ , monochromatic photons,  $\sqrt{s} = 500$  GeV

where  $\epsilon_{\pm}$  is the energy of the  $\mu^{\pm}$ . The asymmetry quantities are mean values of this quantities averaged over all events allowed by cuts. In the future study of effects of New Physics some other variables can be more useful.

We present distributions in these variables in Fig. 14.

For the  $\gamma_-\gamma_-$  and  $\gamma_+\gamma_+$  collisions the distributions in the forward and backward hemispheres are identical. For these initial photon polarizations  $w = 0$  while the variables  $u$  and  $v$  describe interesting asymmetries. Vice versa, for the  $\gamma_-\gamma_+$  collision the distributions in the forward and backward hemispheres can be obtained from each other by the exchange  $\mu^{\pm} \leftrightarrow \mu^{\mp}$ . Therefore, for these collisions  $u = v = 0$  while  $w$  describe the charge asymmetry, see Figure 14.

## VIII. SUMMARY AND OUTLOOK

Let us enumerate main results obtained in this work.

- We consider the *charge asymmetry* of leptons produced together with neutrinos in the collision of polarized photons. This charge asymmetry is defined as the difference in the momentum distributions of the produced negatively and positively charged leptons, and arises be-

cause the CP conserving weak interaction vertex makes the momentum distributions strongly correlated to the initial photon polarization. This asymmetry is observable for each fixed circular polarization of at least one colliding photon.

- In particular, we present a detailed analysis of charge asymmetries, in the SM reactions  $\gamma\gamma \rightarrow W^{\pm}\ell^{\mp} + \nu's$  and  $\gamma\gamma \rightarrow \ell^+\ell^- + \nu's$ , with polarized photons. The method of observation of this effect, described in detail in the text, is based on a standard differential analysis of final state momentum distributions of the observed leptons with suitable applied cuts, and using well known Monte Carlo software for the generation of events.

- We suggest the method for obtaining an estimate of the lower bound for the statistical uncertainty of future experiments as given by the error of the Monte Carlo simulation at the anticipated number of events. We find that this uncertainty for the quantities under interest in our

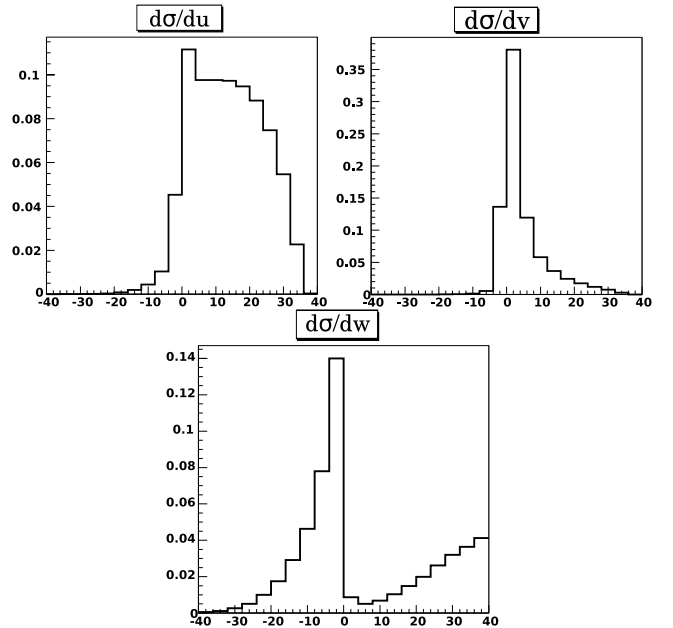


FIG. 14: Distribution in  $u$  (left) and  $v$  (right) for  $\gamma_-\gamma_-$  collision. Bottom: Distribution in  $w$  for  $\gamma_-\gamma_+$  collision. The  $\gamma\gamma \rightarrow \mu^+\mu^-\nu\bar{\nu}$  process with monochromatic photons at  $\sqrt{s} = 500$  GeV

problem is significantly larger than  $1/\sqrt{N}$  (by a factor  $3 \div 5$ ).

- Table I shows that the statistical uncertainty in the charge asymmetry is at the level of radiative corrections. Therefore loop corrections to the differential distributions and the resulting corrections to the charge asymmetries can be safely neglected in the analysis of this type of experiments to be performed at a photon collider. One can hope to observe the effects of radiative corrections only if the luminosity would be enhanced by a factor  $10 \div 100$ .

- Processes with intermediate tau lepton decays (cascade process) do also contribute to the final state with  $\ell^\pm$ . We have constructed an approximation, which describes cascade processes simply (based on the double resonant diagrams for  $W^\pm$  pair production). This approximation describes the contribution from cascade processes to the observable charge asymmetries with high enough accuracy, within the statistical uncertainty of future experiments.

- Taking into account the cascade processes changes the charge asymmetry only weekly, the relative value of this contribution decreases at increasing values of the cut-off momentum  $p_\perp^c$ .

- We have further shown that the non-monochromaticity of photons at Photon Colliders

diminishes the considered asymmetries, but only weekly.

- The substantial reduction of cross sections at increasing values of the cut-off momentum  $p_\perp^c$  above  $M_W/2$  is to be compared with the fact that, on the contrary, the charge asymmetries are affected only slightly by  $p_\perp^c$ . This makes the charge asymmetry a very good candidate as optimal observable for the discovery of New Physics effects in the processes  $\gamma\gamma \rightarrow \ell^+\ell^- + \text{neutrals}$  if, as it is expected, the scale of the New Physics is larger than  $M_W$ .

## Acknowledgments

This work is supported by grants RFBR 08-02-00334-a and NSH-1027.2008.2. I. F. Ginzburg acknowledges support from the *Centro di Cultura Scientifica Alessandro Volta*, Landau Network office, which allowed a visit to INFN Sezione di Perugia, where this work was initiated. This work was also partially supported, in the earlier stages, by the European Contract HPMF-CT-2000-0752. K.Kanishev is supported also by EU Marie Curie Research Training Network FLAVIANet under contract No. MRTN-CT-2006-035482

- 
- [1] B. Badelek *et al.* *Int. J. Mod. Phys. A* **19** (2004) 5097-5186
  - [2] I. F. Ginzburg, G. L. Kotkin, V. G. Serbo and V. I. Telnov, *Nucl. Instrum. Meth.* **205** (1983) 47;  
I. F. Ginzburg, G. L. Kotkin, S. L. Panfil, V. G. Serbo and V. I. Telnov, *Nucl. Instrum. Meth. A* **219** (1984) 5.
  - [3] E. Boos *et al.* *Nucl. Instr. Meth. A* **534** (2004) 250; hep-ph/0403113
  - [4] A. Pukhov, hep-ph/0412191
  - [5] S. Jadach, Z. Was, R. Decker and J. H. Kuhn, *Comput. Phys. Commun.* **76**, 361 (1993).
  - [6] D. A. Anipko, M. Cannoni, I. F. Ginzburg, A. V. Pak, O. Panella, *Nucl. Phys. B Proc. Suppl.* **126** (2004) 354-359; hep-ph/0306138; hep-ph/0410123.
  - [7] E. Boos and T. Ohl, *Phys. Lett. B* **407** (1997) 161, hep-ph/9705374.
  - [8] I.F. Ginzburg, G.L. Kotkin, S.L. Panfil, V.G. Serbo, *Nucl. Phys. B* **228** (1983) 285.
  - [9] M. Baillargeon, G. Belanger and F. Boudjema, *Phys. Lett. B* **404**, 124 (1997)[arXiv:hep-ph/9701368]; *Nucl. Phys. B* **500**, 224 (1997) [hep-ph/9701372]; [hep-ph/9405359].
  - [10] I.F. Ginzburg, G.L. Kotkin. *Eur. Phys. J. C* **13** (2000) 295-300